Geometric Image Registration under Locally Variant Illuminations Using Huber M-estimator

M.M. Fouad, R.M. Dansereau, and A.D. Whitehead

Dept. of Systems and Computer Engineering,
Carleton University, Ottawa, Ontario, Canada, K1S 5B6
{mmafoad,rdanse}@sce.carleton.ca, awhitehe@connect.carleton.ca

Abstract. In this paper, we extend our previous work on presenting a registration model for images having arbitrarily-shaped locally variant illuminations from shadows to multiple shading levels. These variations tend to degrade the performance of geometric registration and impact subsequent processing. Often, traditional registration models use a least-squares estimator that is sensitive to outliers. Instead, we propose using a robust Huber M-estimator to increase the geometric registration accuracy (GRA). We demonstrate the proposed model and compare it to other models on simulated and real data. This modification shows clear improvements in terms of GRA and illumination correction.

1 Introduction

Geometric image registration (GIR) of a set of images is a common pre-processing step in many applications [1], such as super-resolution [2], image stitching [3], and remote-sensing applications [4]. For these and similar applications, sub-pixel accuracy in registration is necessary for satisfactory post-processing results.

Existing image registration approaches can be categorized into feature-based and intensity-based. The former rely on the fact that the extracted features in one image are matched to their corresponding features in another image, either by their appearance similarity or by geometric closeness (see *e.g.*, [5, 6]), or by local descriptors, such as SIFT, Harris, *etc.* (see *e.g.*, [7, 8]). Although these approaches have robustness to outliers, such as RANSAC [9, 10], they can be highly sensitive to the feature extraction process, especially in the presence of locally variant illumination changes [3]. Note that outliers in feature-based registration approaches denotes a mismatch between corresponding features. Another major problem of feature-based approaches is that the sparseness of the features increases the geometric registration error, especially if the features are less dense in a specific part of the input images.

Intensity-based approaches directly deal with image intensity without detecting prominent features. These approaches aim to find a transformation function such that the discrepancy in the intensity of the corresponding pixels are minimized. These approaches avoid some of the pitfalls of the feature extraction stage. Although a number of researchers [11–14] have incorporated global or

A. Elmoataz et al. (Eds.): ICISP 2010, LNCS 6134, pp. 10–18, 2010.

semi-local illumination models into the image registration problem, their approaches do not allow arbitrarily-shaped illumination changes that could occur in real imaging scenarios.

The GIR process is impacted by the presence of locally variant illumination changes [3]. In [11, 12], a global illumination (GI) model is presented to relate the intensity levels of an image pair, where pre-defined neighborhoods with an imposed smoothness constraint are proposed in [11]. In [13], an affine illumination model is given with triangular or quadratical region support. In [14], a dual inverse compositional algorithm is proposed based on the assumption that the geometric and photometric parameters can commute, thereby impeding the use of explicit local intensity transformations. Unfortunately, the resulting registration from these models tends to be degraded when arbitrarily-shaped regions with distinct illumination variations exist.

In our previous work [15], although local illumination variations have been taken into account simultaneously with GIR, one can notice two limitations. First, these variations are limited to two illumination levels (*i.e.*, shadowed and non-shadowed). Second, the approaches in [11–15] use a least-squares estimator (LSE). Intuitively, the LSE is more sensitive to outliers, since its influence function (*i.e.*, the first derivative) is proportional to the residuals' magnitude. Instead, the LSE can be replaced by a function that assigns smaller weights for larger residuals. The most common method is Huber M-estimation [16], that has greater resistance to outliers as it differently penalizes the residuals. Note that outliers in intensity-based registration approaches refers to corresponding pixels that have large absolute intensity difference due to illumination variations.

In this paper, we propose an intensity-based registration approach by extending the approach in [15] to cope with multiple shading levels simultaneously with improving GIR accuracy using a robust Huber M-estimator [16] instead of LSE. Since [13]'s approach tends to limit the illumination regions to predefined shapes, and [14]'s algorithm prevents using local illumination transformations, we compare the proposed model to the ASLIV model presented in [15], and the GI model shown in [11, 12].

This paper is organized as follows. In Section 2, we propose an approach using Huber M-estimator. In Section 3, we develop the experiments using real and simulated data sets. Finally, conclusions are given in Section 4.

2 Proposed Model With Huber M-estimator

In this section, we propose a registration model to improve geometric registration and illumination correction, while using Huber M-estimator.

2.1 Model

Consider that we have two $N \times M$ input images, I_1 and I_2, captured for the same scene at two different times. Both images may have distinct illumination regions

with arbitrary shapes. We can formulate our extended registration model that relates the intensity levels of I_1 and I_2 as the matrices,

$$I_2(\mathbf{x}_2) \simeq B(\mathbf{x}_1)\, I_1(\mathbf{x}_1) + C(\mathbf{x}_1)\,, \tag{1}$$

where $\mathbf{x} = (x, y)$ is a pixel location, and $\{I_i, B, C\} \in \mathbb{R}^{N\times M}$. As presented in [15], the illumination variations, B and C, are modeled as matrices,

$$B = \begin{bmatrix} b_{11} & \dots & b_{1M} \\ \vdots & \ddots & \vdots \\ b_{N1} & \dots & b_{NM} \end{bmatrix},\ C = \begin{bmatrix} c_{11} & \dots & c_{1M} \\ \vdots & \ddots & \vdots \\ c_{N1} & \dots & c_{NM} \end{bmatrix}. \tag{2}$$

Many motion models could be used to model the motion in (1). However, we chose the 6-parameter affine motion model as shown in [11–13, 15] (*i.e.*, $\mathbf{x}_2 = A(\mathbf{x}_1)$, see Eqs. (3) and (4) in [15]). In addition, in [15], the illumination changes were limited to two shading levels. In this paper, the approach is generalized such that each image I_i can contain V_i distinct levels of illumination.

To demonstrate the idea of the proposed model, we will start with the case that *a priori* known information of distinct shading levels is available. Fig. 1(a) shows an example of a masked image I_1 segmented into three distinct illumination levels: L_1^1, L_1^2 and L_1^3 (*i.e.*, V_1=3). Similarly, Fig. 1(b) depicts another masked image I_2 segmented, as well, into a different set of distinct illumination levels: L_2^1, L_2^2 and L_2^3 (*i.e.*, V_2=3). With a rough geometric registration for I_1 and I_2, an absolute image difference (AID), $I_{1,2}$, is created having a set of overlapping regions, R_j, such that $I_{1,2} = \bigcup_{j=1}^{J} R_j$ (see Fig. 1-c), where J refers to the number of resulting overlapping regions. Similarly, in a real imaging scenario, we propose a simple method of segmenting the AID of the roughly aligned images using, for instance, the k-means algorithm [17]. Thus, the illumination regions, R_j, are obtained: first estimated and then iteratively refined.

Note that the sum of the number of distinct illumination levels in both images (*i.e.*, $V_1 + V_2$) does not express the number of the resultant overlapping regions, J, as the latter depends on the former as well as the intersections among these distinct levels, $L_i^v\ \forall v$. We'd like to stress that each resulting region, R_j, is assumed to have its own constant brightness b_j and contrast c_j. A special case was discussed in [15], where $J = 2$.

For pixel domain mathematical manipulations, each R_j can be represented by a binary mask, $Q_j(\mathbf{x})$, such that

$$Q_j(\mathbf{x}) = \begin{cases} 1, \forall\ \mathbf{x} \in R_j \\ 0, \text{otherwise} \end{cases}, \quad \text{where } Q_j \in \mathbb{R}^{N\times M}. \tag{3}$$

Thus, we can constrain B and C in (1) to J regions as follows

$$B = \sum_{j=1}^{J} b_j Q_j\,, \quad C = \sum_{j=1}^{J} c_j Q_j\,. \tag{4}$$

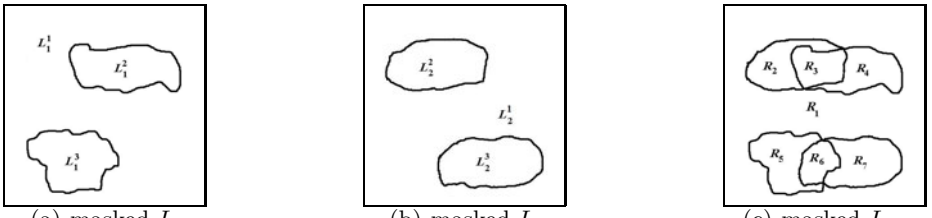

(a) masked I_1 (b) masked I_2 (c) masked $I_{1,2}$

Fig. 1. With *a priori* known information, (a,b) two different sets of distinct illumination levels of two input images (*i.e.*, V_1=V_2=3), yielding (c) a masked AID with seven arbitrarily-shaped regions, each has its own constant illumination (*i.e.*, J=7).

The following section presents an approach to estimate the unknown vector $\mathbf{\Phi} = [a_1, \ldots, a_6, b_1, \ldots, b_J, c_1, \ldots, c_J]^\top$, which contains the 6 parameters of affine motion, J for brightness and J for contrast, respectively.

2.2 Iterative Scheme Using Huber M-estimator

This section presents an iterative framework using Huber M-estimator in order to estimate the unknown vector $\mathbf{\Phi}$. Unlike the quadratic cost function presented in [11–13, 15], we propose using Huber M-estimator [16]

$$\min_{\mathbf{\Phi}} \left\{ \mathcal{L} = \sum_{\mathbf{x}} \Psi(E(\mathbf{\Phi}, \mathbf{x}); \alpha) \right\}, \quad \text{where } \Psi(t;\alpha) = \begin{cases} \frac{1}{2}t^2, & |t| \leq \alpha \\ \alpha|t| - \frac{1}{2}\alpha^2, & |t| > \alpha \end{cases}, \quad (5)$$

where α is a positive tuning threshold, $\Psi(\cdot)$ denotes Huber's function, and $E(\mathbf{\Phi}, \mathbf{x})$ refers to the residual located at position $\mathbf{x} = (x, y)$. This Huber M-estimation formula can be rewritten [18] as

$$\min_{\mathbf{\Phi}} \left\{ \mathcal{L} = 0.5 \sum_{\mathbf{x}} \left[E^2(\mathbf{\Phi}) \cdot F + 2\,\alpha\, S \cdot E(\mathbf{\Phi}) - \alpha^2 \right] \right\}, \quad (6)$$

where $(\cdot)$ refers to element-by-element matrix product. The residuals can be expressed as

$$E(\mathbf{\Phi}; \mathbf{x}) = I_2(A(\mathbf{x})) - B(\mathbf{x})\, I_1(\mathbf{x}) - C(\mathbf{x})\,. \quad (7)$$

The high-residual selective matrix is

$$S = \begin{bmatrix} s_{11} & \cdots & s_{1M} \\ \vdots & \ddots & \vdots \\ s_{N1} & \cdots & s_{NM} \end{bmatrix}, \quad s_{xy} = \begin{cases} -1, & E(\mathbf{\Phi}; \mathbf{x}) < -\alpha \\ 0, & |E(\mathbf{\Phi}; \mathbf{x})| \leqslant \alpha \\ 1, & E(\mathbf{\Phi}; \mathbf{x}) > \alpha \end{cases}. \quad (8)$$

While, the low-residual selective matrix is

$$F = \mathbf{1} - S \cdot S, \quad f_{xy} = 1 - s_{xy}^2\,, \quad (9)$$

where f_{xy} is an element of F at position (x, y), and $\{\mathbf{1},\, E,\, S,\, F\} \in \mathbb{R}^{N\times M}$. We can estimate $\mathbf{\Phi}$ using the Gaussian-Newton method [20] to solve the non-linear minimization problem in (6). Note that $\hat{\mathbf{\Phi}}$ is updated by $\mathbf{\Delta}$ at each iteration k, such that $\hat{\mathbf{\Phi}}_k = \hat{\mathbf{\Phi}}_{k-1} + \mathbf{\Delta}_k$.

Replacing $E(\cdot)$ in (7) by its 1^{st} order Taylor series expansion, then F in (6) can be rewritten as

$$\mathcal{L} = 0.5 \sum_{\mathbf{x}} \Big[F \cdot \big(E(\mathbf{\Phi}_{k-\mathbf{1}}) + \mathbf{\Delta}_k^\top \nabla_{\mathbf{\Phi}} E(\mathbf{\Phi}_{k-\mathbf{1}}) \big)^2 + 2\,\alpha\, S \cdot \big(E(\mathbf{\Phi}_{k-\mathbf{1}}) + \mathbf{\Delta}_k^\top \nabla_{\mathbf{\Phi}} E(\mathbf{\Phi}_{k-\mathbf{1}}) \big) - \alpha^2 \Big]. \quad (10)$$

Setting the gradient of $\mathcal{L}$ w.r.t. $\mathbf{\Delta}$ to zero, we obtain

$$-\sum_{\mathbf{x}} \left[(E(\mathbf{\Phi}_{k-\mathbf{1}})\, \nabla_{\mathbf{\Phi}} E(\mathbf{\Phi}_{k-\mathbf{1}})) \cdot F + \alpha\, S \cdot \nabla_{\mathbf{\Phi}} E(\mathbf{\Phi}_{k-\mathbf{1}}) \right] = \hat{\mathbf{\Delta}}_k^\top \sum_{\mathbf{x}} \left[\big(\nabla_{\mathbf{\Phi}} E(\mathbf{\Phi}_{k-\mathbf{1}})\, \nabla_{\mathbf{\Phi}} E^\top (\mathbf{\Phi}_{k-\mathbf{1}}) \big) \cdot F \right]. \quad (11)$$

We can write (11) in matrix notation as

$$-\mathbf{Y}\ \mathbf{P}^\top = (\mathbf{Y}\ \mathbf{H}^\top)\ \hat{\mathbf{\Delta}}, \quad (12)$$

where

$$\mathbf{H} = [H_{11}, H_{12}, \ldots, H_{pq}],\ \mathbf{Y} = [Y_{11}, Y_{12}, \ldots, Y_{pq}],\ \mathbf{P} = [P_{11}, P_{12}, \ldots, P_{pq}],$$

$$H_{pq} = [pI_x, qI_x, pI_y, qI_y, I_x, I_y, -I_1Q_1, \ldots, -I_1Q_J, -Q_1, \ldots, -Q_J]^\top, \quad (13)$$

$$Y_{pq} = f_{pq}\ [pI_x, qI_x, pI_y, qI_y, I_x, I_y, -I_1Q_1, \ldots, -I_1Q_J, -Q_1, \ldots, -Q_J]^\top, \quad (14)$$

$$\text{and} \qquad P_{pq} = \alpha\ s_{pq} + f_{pq}\ I_2(p,q)\ , \qquad 1 \leqslant p, q \leqslant N, M. \quad (15)$$

Equations (12) through (15) can be used to perform one iteration for finding a solution of $\hat{\mathbf{\Delta}}$ to update $\hat{\mathbf{\Phi}}$. As well, our approach uses a coarse-to-fine [19] framework to cope with large motions with r resolution levels. The convergence is achieved at the last resolution level, when either the cost function in (6) is updated by less than a predefined threshold, ε, or a maximum number of iterations, k, has been reached. The unknown parameters at each iteration are accumulated yielding a single final estimate. We will refer to the proposed model explained in this section by HM-ASLIV$_{6,2J}$, where the superscript accounts for the $6{+}2J$ parameters in $\mathbf{\Phi}$.

3 Experimental Results

In this section, we develop the experiments and compare the proposed model HM-ASLIV to the ASLIV model in [15] and the GI model in [11, 12], whose implementation can be found online [22].

Table 1. The AAE ($\times 10^{-4}$) of the estimated affine parameters of the *"J=3"* and *"J=4"* data computed by the competing models compared to their ground truth values

	"J=3" data set			*"J=4"* data set		
Para.	GI	$\text{ASLIV}_{6,6}$	$\text{HM-ASLIV}_{6,6}$	GI	$\text{ASLIV}_{6,8}$	$\text{HM-ASLIV}_{6,8}$
a_1	15.3658	1.7205	**1.2025**	16.5962	1.8021	**1.4358**
a_2	12.0018	1.5079	**1.0344**	13.2015	1.6025	**1.1916**
a_3	14.6081	1.6189	**1.1661**	15.5246	1.7360	**1.2049**
a_4	19.1128	2.0502	**1.8699**	21.0259	2.4261	**1.9280**
a_5	9190.77	789.16	**722.35**	9472.09	816.50	**760.57**
a_6	2688.72	795.70	**716.11**	2835.12	804.81	**755.11**

Table 2. SSIM indexes, PSNR and NCC values express the correlation between the overlapping region of the registered pairs for a random subset of the *"J=3"* data set using (i) GI, (ii) $\text{ASLIV}_{6,6}$ and (iii) $\text{HM-ASLIV}_{6,6}$ models

	SSIM [23]			PSNR (dB)			NCC [24]			Time (sec.)		
Pair #	(i)	(ii)	(iii)	(i)	(ii)	(iii)	(i)	(ii)	(iii)	(i)	(ii)	(iii)
10	0.8397	0.9602	**0.9622**	22.53	29.02	**29.78**	0.9111	0.9942	**0.9956**	43.0	57.7	**62.2**
17	0.8194	0.9577	**0.9589**	20.01	28.33	**29.01**	0.9241	0.9932	**0.9948**	42.8	55.4	**59.8**
28	0.8268	0.9534	**0.9598**	21.76	29.42	**30.17**	0.9049	0.9939	**0.9951**	44.7	58.8	**61.4**
34	0.8066	0.9507	**0.9531**	21.91	27.01	**27.76**	0.9100	0.9927	**0.9946**	43.3	57.2	**62.5**
38	0.8552	0.9650	**0.9665**	23.47	28.63	**29.25**	0.9192	0.9948	**0.9956**	42.7	56.4	**63.2**
48	0.8419	0.9634	**0.9643**	21.94	29.69	**30.10**	0.9067	0.9941	**0.9953**	41.2	55.3	**59.4**

Table 3. NCC for the real pairs using GI, $\text{ASLIV}_{6,8}$ and $\text{HM-ASLIV}_{6,8}$ models

Pair	GI	$\text{ASLIV}_{6,8}$	$\text{HM-ASLIV}_{6,8}$	Pair	GI	$\text{ASLIV}_{6,8}$	$\text{HM-ASLIV}_{6,8}$
A	0.8819	0.9226	**0.9237**	E	0.9601	0.9743	**0.9758**
B	0.9642	0.9789	**0.9802**	F	0.9919	0.9922	**0.9939**
C	0.9799	0.9853	**0.9870**	G	0.9651	0.9657	**0.9671**
D	0.9550	0.9644	**0.9659**	H	0.9071	0.9229	**0.9245**

3.1 Data Set Description and Performance Evaluation

The image data sets used in the experiments include two categories: real and simulated. The first category involves nine real 400×400 and 600×600 LANDSAT satellite images [21] with unknown true motion. The second category includes 50 simulated image pairs that are 500×500 pixels acquired from 3000×3000 pixel IKONOS satellite images for the Pentagon and its surroundings as shown in [15]. Each simulated pair is subjected to varying V_1 and V_2 levels of illumination, respectively, in different areas in both images according to the desired number of illumination regions J; set to 3 and 4. Note that all the simulated pairs are directly presented to competing models without pixel quantization error.

For the real and simulated data sets, we determine the correlation between the overlapping area of the two registered images using commonly used image

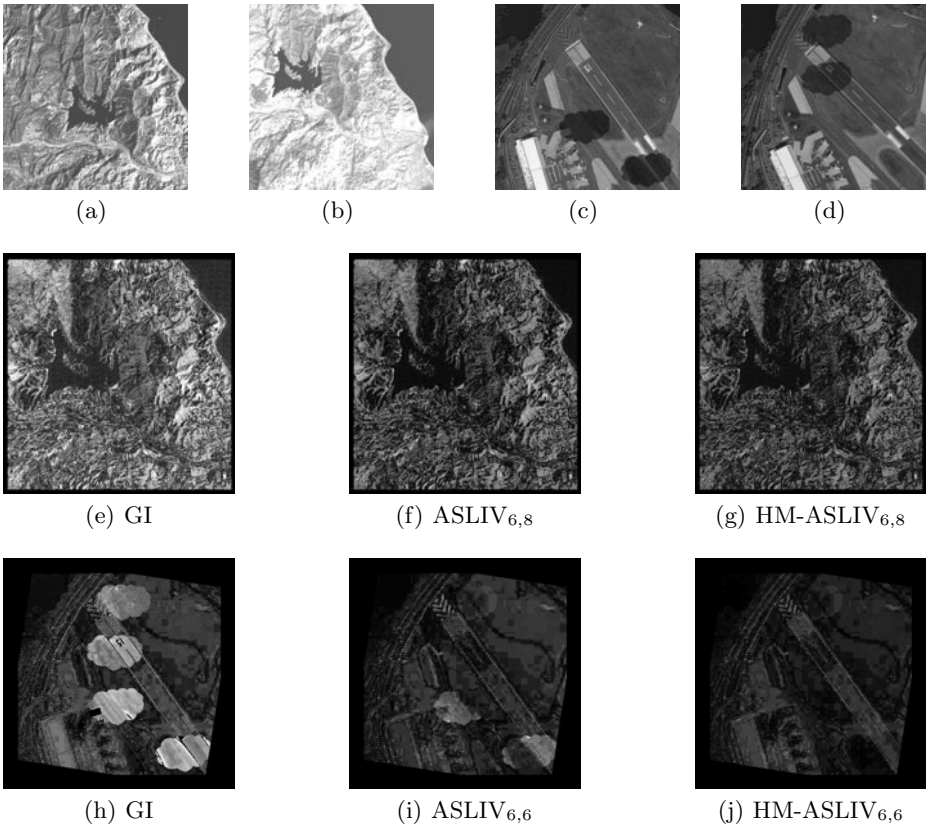

Fig. 2. (a,b) A real pair (#B). (c,d) A "J=3" simulated pair (#34). Using the competing models, (e,f,g) gamma-corrected AIDs of the real pair in (a,b), $\gamma = 1.7$, with NCC=0.9642, 0.9789 and 0.9802, respectively, and (h,i,j) normalized AIDs of the simulated pair in (c,d), with PSNR=21.91, 27.01 and 27.76 dB, respectively.

quality measures: structure similarity (SSIM) index [23], PSNR (in dB) and normalized cross-correlation (NCC) [24]. The average of absolute error (AAE) between the estimated affine parameters and the corresponding ground truth values is also computed for the simulated data sets.

3.2 Implementation Setup and Discussion

Our implementation runs on a 2 GHz Pentium IV Core 2 Duo, with 2 GB of RAM. We compare the HM-ASLIV model to the GI model in [11, 12] and that in [15]. We will refer to the model in [15] by ASLIV$_{6,2J}$, in which the quadratic cost function is employed, but for J=3 and 4 (*i.e.*, ASLIV$_{6,6}$ and ASLIV$_{6,8}$, respectively). In our experiments, an identity initialization is used for $\mathbf{\Phi}^{\circ}$ yielding an initial guess that the two input images are aligned and no illumination variations exist. Thus, $\mathbf{\Phi}^{\circ}$ is either set to $[1, 0, 0, 1, 0, 0, 1, 1, 1, 0, 0, 0]$ with mod-

els $\text{ASLIV}_{6,6}$ and $\text{HM-ASLIV}_{6,6}$ or set to $[1,0,0,1,0,0,1,1,1,1,0,0,0,0]$ using models $\text{ASLIV}_{6,8}$ and $\text{HM-ASLIV}_{6,8}$. Our approach iteratively exploits a coarse-to-fine framework with 5 resolution levels (*i.e.*, r=5), so that $\hat{\mathbf{\Phi}}$ is adequately estimated at the coarsest level for both real and simulated data. For convergence settings, ε and k are set to 0.1 and 10, respectively. Note that α is set to $1.345\,\sigma$ [20] when using the HM-ASLIV model, where σ is the standard deviation of the residuals computed at each iteration.

Table 1 shows that the proposed model, HM-ASLIV, provides more precise motion estimates, in the presence of local illumination variations, over GI and ASLIV models for the *"J=3"* and *"J=4"* data sets. In addition, Tables 2 and 3 show that the selected image quality measures using the proposed model, HM-ASLIV, outperform those using the GI and ASLIV models with a slight increase in computational time using simulated and real data.

The gamma-corrected AIDs of the registered pairs, of the pair in Fig. 2-(a,b), are manifested in Fig. 2-(e,f,g) using GI, $\text{ASLIV}_{6,8}$ and $\text{HM-ASLIV}_{6,8}$ models, respectively ($\gamma = 1.7$ for better visualization). Similarly, the normalized AIDs of the aligned pairs, for the pair in Fig. 2-(c,d), are shown in Fig. 2-(h,i,j) using GI, $\text{ASLIV}_{6,6}$ and $\text{HM-ASLIV}_{6,6}$ models, respectively. Since the less the brightness, the more precise the GRA, Fig. 2 shows that the HM-ASLIV model qualitatively outperforms both GI and ASLIV models.

4 Conclusions

In this paper, we present an intensity-based image registration model to cope with images having multiple illumination variations (regions) with arbitrary shapes. The proposed model assumes brightness and contrast uniformity within each illumination region, which allows conditioning of the ill-posed problem. The approach also uses a robust Huber M-estimator that is not as vulnerable as LSE to outliers. Convergence is well achieved with an identity initialization, through an iterative coarse-to-fine scheme to allow for large motions. The experiments are performed on both real and simulated data sets. Clear improvements in terms of geometric registration accuracy are obtained using the proposed model as opposed to the GI model [11, 12] and ASLIV model [15] by an average increase of 88.5% and 18.9%, respectively, with only a slightly average increase of 33.1% and 11.6%, respectively, in computational time.

References

1. Zitová, B., Flusser, J.: Image registration methods: A Survey. Image & Vis. Comp. 21, 977–1000 (2003)
2. Gevrekci, M., Gunturk, B.: Superresolution under photometric diversity of images. Advances in Signal Proc. (2007)
3. Szeliski, R.: Image alignment and stitching: A tutorial. Found. and Trends in Comp. Graphics and Vision 2 (2006)
4. Lou, L., Zhang, F., Xu, C., Li, F., Xue, M.: Automatic registration of aerial image series using geometric invariance. In: IEEE ICAL, pp. 1198–1203 (2005)

5. Aylward, S., Jomier, J., Weeks, S., Bullitt, E.: Registration of vascular images. Comp. Vis. 55, 123–138 (2003)
6. Xu, D., Kasparis, T.: Robust image registration under spatially non-uniform brightness changes. In: IEEE ICASSP, vol. 2, pp. 945–948 (2005)
7. Ke, Y., Sukthankar, R.: PCA-SIFT: a more distinctive representation for local image descriptors. Comp. Vis. and Patt. Recog. 2, 506–513 (2004)
8. Battiato, S., Gallo, G., Puglisi, G., Scellato, S.: SIFT features tracking for video stabilization. In: Proc. 14th ICIAP, pp. 825–830 (2007)
9. Fischler, M., Bolles, R.: Random Sample Consensus: a paradigm for model fitting with applications to image analysis and automated cartography. Comm. Of the ACM 24, 381–395 (1981)
10. Hartley, R., Zisserman, A.: Multiple view geometry in computer vision, 2nd edn. Cambridge University Press, Cambridge (2003)
11. Periaswamy, S., Farid, H.: Elastic registration in the presence of intensity variations. IEEE Trans. Med. Imag. 22, 865–874 (2003)
12. Aguiar, P.: Unsupervised simultaneous registration and exposure correction. In: IEEE ICIP, pp. 361–364 (2006)
13. Altunbasak, Y., Mersereau, R., Patti, A.: A fast parametric motion estimation algorithm with illumination and lens distortion correction. IEEE Trans. Image Proc. 12, 395–408 (2003)
14. Bartoli, A.: Groupwise geometric and photometric direct image registration. IEEE Trans. Patt. Ana. & Mach. Intel. 30, 2098–2108 (2008)
15. Fouad, M., Dansereau, R., Whitehead, A.: Geometric registration of images with arbitrarily-shaped local intensity variations from shadows. In: IEEE ICIP, pp. 201–204 (2009)
16. Huber, P.: Robust Statistics, 1st edn. Wiley, New York (1981)
17. Kanungo, T., Mount, D., Netanyahu, N., Piatko, C., Silverman, R.: An efficient *K*-means clustering algorithm: Analysis and implementation. IEEE Trans. Patt. Ana. & Mach. Intel. 24, 881–892 (2002)
18. Mangasarian, O., Musicant, D.: Robust linear and support vector regression. IEEE Trans. Patt. Ana. & Mach. Intel. 22, 950–955 (2000)
19. Jiang, J., Zheng, S., Toga, A., Tu, Z.: Learning based coarse-to-fine image registration. In: IEEE ICCVPR, pp. 1–7 (2008)
20. Nocedal, J., Wright, S.: Numerical optimization. Springer, New York (1999)
21. `http://vision.ece.ucsb.edu/registration/satellite/` (accessed January 2009)
22. `http://users.isr.ist.utl.pt/~aguiar/mosaics/` (accessed January 2009)
23. Wang, Z., Bovik, A., Sheikh, H., Simoncelli, E.: Image quality assessment: From error visibility to structural similarity. IEEE Trans. Image Proc. 13, 600–612 (2004)
24. Barnea, D., Silverman, H.: A class of algorithms of fast digital image registration. IEEE Trans. Comp. 21, 179–186 (1972)